Alignment-resolved O$_2$ scattering from highly oriented pyrolytic graphite and LiF(001) surfaces

Mitsunori Kurahashi[1] and Takahiro Kondo[2]

[1]*National Institute for Materials Science, 1-2-1 Sengen, Tsukuba, Ibaraki 305-0047, Japan*
[2]*Faculty of Pure and Applied Sciences, University of Tsukuba, 1-1-1 Tennoudai, Tsukuba, Ibaraki 305-8573, Japan*

We present an alignment-resolved O$_2$ scattering experiment showing that the alignment of an incident homonuclear diatomic molecule strongly influences the angular distribution of scattered molecule, the energy loss during the collision, and the trapping probability. Clear surface rainbow scattering has been observed on LiF(001) when O$_2$ is scattered along the [110] azimuth with its axis perpendicular to the scattering plane. The results can be understood based on the alignment dependence of the surface corrugation felt by an incident molecule. The fact that O$_2$ trapping probability on a highly oriented pyrolytic graphite surface is higher for end-on collision has been associated with the observed larger energy loss for this geometry.

I. INTRODUCTION

State-resolved molecular beam-surface scattering experiments, which specify the geometry and internal states of incident and/or scattered molecules, provide valuable information not only on the geometrical effect in the molecule-surface interaction, but also on the mechanism of energy dissipation of impinging molecules necessary to result in trapping or chemisorption [1–6]. The geometrical effect here is usually classified into two categories. One is the *orientation* effect and the other is the *alignment* effect. The effect of orientation, i.e., the head-to-tail direction of an incident heteronuclear molecule, on its interaction with surfaces has been investigated for several polar molecule-surface systems [7–15]. It has been shown that, for NO scattering from flat metallic surfaces, the observed orientation dependence in the angular distribution and the rotational excitation of scattered molecules [10–13] can be understood based on the orientation dependent molecule-surface interaction potential [14,15].

In contrast, experimental studies concerning the alignment effect, which is associated with the difference between "side-on" and "end-on" collisions, have been limited to the chemisorption studies [16–18] and that for ion-surface interaction [19]. Its effect on nonreactive molecule-surface scattering however remains mostly unexplored. Unlike the scattering of heteronuclear molecules where the orientation effect is dominant, alignment would be the key factor in the scattering of heavy homonuclear molecules, such as O$_2$, N$_2$, etc. These molecules have an elongated shape and their dimensions [20] are often comparable to the spatial period of surface corrugation. It is therefore expected that, depending on the alignment relative to the surface, the direction of the forces acting on the incident molecule and/or the surface corrugation felt by it can be largely different, possibly affecting the angular distribution of scattered molecules and the energy dissipation processes. This may be closely related to the fact that non-state-resolved polyatomic molecule-surface scattering experiments on a LiF(100) surface show structure-less angular distributions [21,22], while atom [22,23] or small

spherical molecule [24] scattering on it exhibits clear surface rainbow scattering. Kondo *et al.* [22], based on the simulation with the ellipsoid washboard model, have associated this with the averaged contribution of differently aligned molecules contained in the randomly oriented beam used. To the best of our knowledge, however, surface scattering experiments with a beam of aligned heavy homonuclear molecules necessary to clarify this issue have not been reported yet.

In this paper, we present experimental evidence showing that the alignment of O$_2$ affects the angular distribution of scattered molecule, the trapping probability, and the energy dissipation efficiency. We also demonstrate that the surface rainbow scattering does appear if the collision occurs at a geometry where O$_2$ can feel the surface corrugation effectively.

II. EXPERIMENT

The alignment-resolved O$_2$ scattering experiments have been conducted with a single spin-rotational state-selected [$(J, M) = (2, 2)$] O$_2$ beam [17,25]. The state-selected O$_2$ beam was prepared by passing a supersonic seeded O$_2$/He beam through a hexapole magnet. Here, the magnetic hexapolar field was used as a filter to transmit the (2,2) state and reject others. The translational energy (E_0) of the O$_2$ (2,2) beam was controlled in the energy range of 0.08–0.25 eV by adjusting the length of the hexapole and the velocity of the seeded O$_2$ beam. The intensity of O$_2$ molecules scattered or desorbed from the crystal, which is rotatable along the axis perpendicular to the scattering plane, was measured by a differentially pumped mass spectrometer equipped at a fixed angle of 45° relative to the incidence beam [Fig. 1(a)]. The sum of the incidence angle (θ_i) and scattering angle (θ_f) relative to the surface normal is therefore 45°. Since the rotational quantum numbers for the $(J, M) = (2, 2)$ state are specified to be $(K, M_K) = (1, 1)$, the O$_2$ axis angular distribution function is given by $|Y_1^1|^2$ ($= \frac{3}{8\pi}\sin^2\alpha$), where α is the polar angle of the molecular axis relative to the defining magnetic field (H) direction [16,17,25].
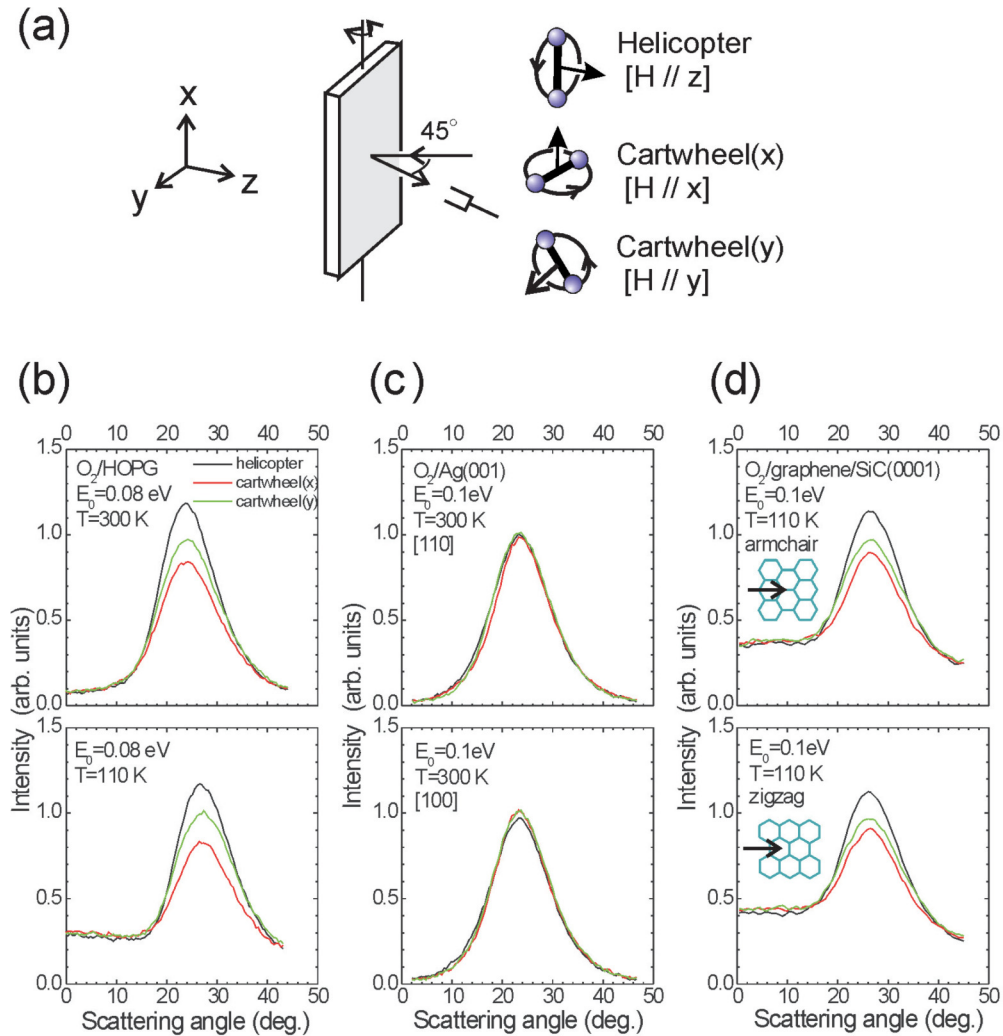
FIG. 1. (a) Three different geometries of incident O_2 used for the scattering experiment. (b)–(d) The angular intensity distributions of O_2 molecules scattered from (b) HOPG, (c) Ag(001), and (d) graphene/SiC(0001) surfaces. The translational energy, the sample temperature, and the azimuth along which the scattering was monitored are shown in the figures. The scattering spectra are normalized to the main peak intensity at $20°$–$30°$ for random orientation, which is the average for the three geometries.

The scattering experiments were conducted at helicopter and two nonequivalent cartwheel geometries shown in Fig. 1(a). In helicopter geometry, where H is along the surface normal (z direction), the molecular axis of incident O_2 is mainly parallel to the surface. Two cartwheel geometries, where H is parallel to the surface, contain contributions of perpendicular molecules, but these two are different in that the rotational axis is perpendicular (parallel) to the scattering plane in cartwheel (x) [cartwheel (y)] geometries. The H direction was changed following the incidence angle scan during the measurement. The fluctuation of the beam and detector conditions was less than 1%. We note that the rotational energy for the O_2 (2, 2) state is 0.36 meV [17], which is much lower than the E_0 values used in the present study. This means that, since the time scale for translational motion is much faster than a rotational period, incident rotational motion is almost frozen during the molecule's final approach to the surface. In such a situation, alignment of incident O_2 is much more important than its rotational motion.

A highly oriented pyrolytic graphite (HOPG) substrate (ZYA-grade, Panasonic), after being cleaved in the air, was annealed up to 873 K in the ultrahigh vacuum chamber to prepare its clean surface. The epitaxial graphene was prepared on a Si-terminated (0001) face of 6H-SiC by heating the substrate at 1400 °C for 10 min. A low energy electron diffraction (LEED) pattern of the surface (Fig. 2) was similar to that reported in Ref. [26]. The ratio of the intensity of C-270 eV and Si-90 eV Auger peaks at 3 keV incident energy was 13:1, from which the thickness of the graphite layers was estimated to be about 3 monolayers. A LiF(001) substrate cleaved from a bulk single crystal block was annealed at 723 K for a few hours to obtain a well-ordered surface, which has been checked by low energy electron diffraction measurements. A clean Ag(001) surface was prepared by repeating the annealing at 700 K and Ar^+ sputtering at 500 eV.

The intensity of scattered O_2 or He was monitored with a lock-in technique by modulating the primary beam with a 50% duty-cycle chopper. The ion source of the mass spectrometer was magnetically shielded to avoid the effect of the change in
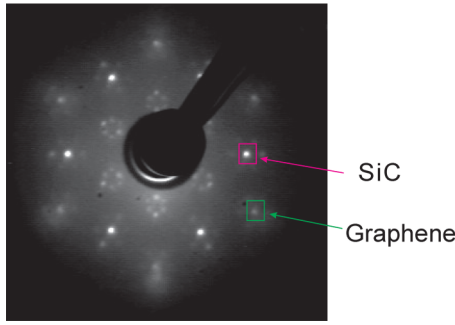
FIG. 2. Low energy electron diffraction pattern from graphene/SiC(0001) measured at the beam energy of 100 eV.

the defining magnetic field direction on the ionization yield. Since a small amount of O$_2$ was accumulated during the scattering measurement on Ag(001), the Ag(001) substrate was annealed shortly at 700 K after each measurement to recover the clean surface.

III. RESULTS AND DISCUSSIONS

A. Direct inelastic scattering of O$_2$ from HOPG

Figure 1(b) shows the angular intensity distribution of O$_2$ molecules scattered or desorbed from an HOPG surface measured at the three geometries. The peak at $\theta_f = 20°–30°$ is associated with direct inelastic scattering following the previous O$_2$ scattering study on HOPG [27]. The peak intensity depends strongly on the geometry, and this dependency is larger at lower temperature. It also shows a broad background-like feature, which has a higher intensity at lower temperature and at around the surface normal ($\theta_f = 0°$). As will be shown later, it attenuates steeply with increasing E_0. This feature can therefore be attributed to trapping followed by desorption.

To see the effect of surface corrugation and orientation of graphite domain relative to the scattering plane, we conducted the same experiments on Ag(001) [Fig. 1(c)] and an epitaxial graphene prepared on SiC(0001) [Fig. 1(d)]. The O$_2$ scattering experiments from Ag(001), which is more flat, along the [110] and [100] azimuths show much weaker geometry dependences, suggesting that surface corrugation would be the main cause of the geometry dependence observed for O$_2$/HOPG. The O$_2$ scattering experiments on the graphene along armchair and zigzag directions show similar geometry dependencies, indicating that the orientation of the graphite domain relative to the scattering plane has little effect on the observed geometry dependence. The geometry dependence observed for the graphene is weaker than that for HOPG, which is probably due to the poorer quality of the present graphene surface. Actually, although the angular width of the specularly reflected He intensity for HOPG was ∼1.5°, which is close to the acceptance angle of the detector aperture, it was ∼4° for the graphene. We therefore use the results for HOPG in the following analysis.

To clarify the origin of the observed alignment effect, the measured scattering/desorption spectra were decomposed into those for the O$_2$ axis angular distribution functions $\rho_x = \frac{3}{4\pi}\sin^2\theta\cos^2\phi$, $\rho_y = \frac{3}{4\pi}\sin^2\theta\sin^2\phi$, and $\rho_z = \frac{3}{4\pi}\cos^2\theta$ [Fig. 3(a)], where θ and ϕ are the polar and azimuth angles
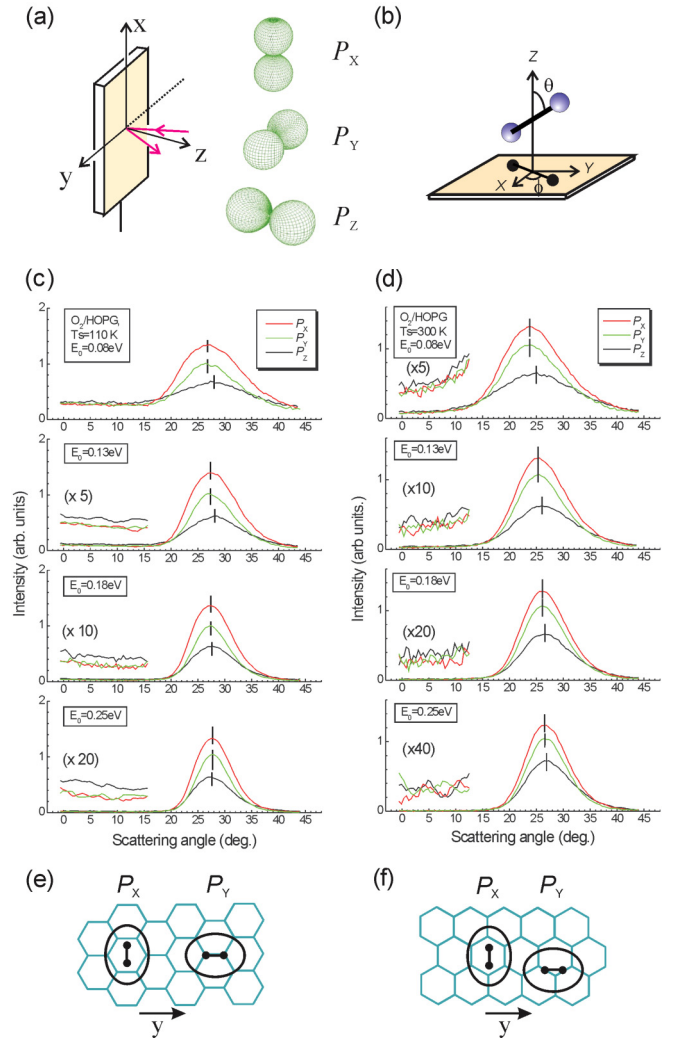

FIG. 3. (a) O$_2$ axis angular distribution functions for P_X, P_Y, and P_Z geometries. O$_2$ is scattered within the yz plane. (b) The definition of the angles representing the O$_2$ axis direction. (c),(d) The angular intensity distributions of O$_2$ scattered from an HOPG surface at (c) 110 K and (d) 300 K derived for the P_X, P_Y, and P_Z geometries. The scattering spectra are normalized to the main peak intensity at 20°–30° for random orientation. The low θ_f part of the spectra that have been rescaled and smoothed by the simple moving average are also shown. (e),(f) Comparison of the P_X and P_Y geometries for the O$_2$ scattering from graphite along (e) armchair and (f) zigzag directions.

of O$_2$ axis relative to the xyz coordinates [Fig. 3(b)]. The O$_2$ axis is distributed mainly along x, y, and z axes in ρ_x, ρ_y, and ρ_z, respectively, and these geometries are denoted as P_X, P_Y, and P_Z [Fig. 3(a)]. Linear combinations of the measured spectra [Fig. 1(b)] allow this decomposition since the distribution functions for the helicopter, cartwheel (x), and cartwheel (y) geometries are equal to $\frac{1}{2}(\rho_x + \rho_y)$, $\frac{1}{2}(\rho_y + \rho_z)$, and $\frac{1}{2}(\rho_x + \rho_z)$, respectively.

The spectra derived for P_X, P_Y, and P_Z geometries [Figs. 3(c) and 3(d)] show the O$_2$ alignment effect more clearly. First, the intensity of the in-plane direct inelastic scattering is in the order of $I(P_X) > I(P_Y) > I(P_Z)$. Second, its peak width is in the order of $\Delta\theta_f(P_Z) > \Delta\theta_f(P_X) > \Delta\theta_f(P_Y)$.

TABLE I. Position (θ_p), the full width at half maximum ($\Delta\theta_f$), and the relative intensity (I_D) of the peak due to the direct inelastic scattering of O_2 from HOPG at 110 K for P_X, P_Y, and P_Z geometries. The relative intensity of the trapping followed by desorption (I_{TD}) is also shown.

E_0 (eV)	P_X				P_Y				P_Z			
	θ_p (deg)	$\Delta\theta_f$ (deg)	I_D	I_{TD}	θ_p (deg)	$\Delta\theta_f$ (deg)	I_D	I_{TD}	θ_p (deg)	$\Delta\theta_f$ (deg)	I_D	I_{TD}
0.08	26.8	12.3	1.10	0.25	26.7	10.8	0.74	0.26	27.9	12.5	0.37	0.30
0.13	27.5	10.1	1.33	0.084	27.2	9.2	0.92	0.085	28.2	10.7	0.50	0.11
0.18	27.3	8.7	1.35	0.032	27.3	7.9	0.95	0.034	27.6	9.3	0.59	0.045
0.25	27.7	7.9	1.32	0.018	27.7	7.2	1.01	0.019	27.5	8.5	0.60	0.028

These observed tendencies are similar over all the experimental range of energies used in this work. Third, the peak position for end-on collision (P_Z geometry) is shifted by $\sim 1°$ to higher θ_f than that for side-on collision (P_X and P_Y geometries) at $E_0 = 0.08$ eV. This peak position shift decreases with increasing E_0 and almost disappears at $E_0 = 0.25$ eV. This behavior is observed both at 110 K and 300 K. Tables I and II summarize the geometry dependence of the peak position, width and intensity of O_2 scattering/desorption from HOPG at 110 K and 300 K, respectively. The parameters shown were derived by fitting the spectra to a Gaussian function $I_D \exp[-(\theta_f - \theta_p)^2/2w^2] + I_{TD}$. The values of I_D and I_{TD} reflect the relative intensities of the direct inelastic scattering and the trapping followed by desorption, respectively. I_{TD} values at 300 K are not shown since the contribution of the trapping followed by desorption is not clear at 300 K.

The alignment dependence of in-plane direct inelastic scattering from HOPG can be understood based on the fact that surface corrugation felt by an incident O_2 molecule depends on the O_2 alignment relative to the surface. On an HOPG surface, valence electron density is higher above the C-C bond of a benzene ring than above the center of the ring, causing the corrugation of the O_2-surface interaction potential. Here, the distance between neighboring benzene ring is ~ 2.5 Å, while O_2 is an ellipsoidal molecule with a length of 4.2 Å and a width of 3.2 Å, which have been estimated based on the computed charge analysis [20].

To discuss the origin of the geometry dependence of the in-plane direct scattering, two types of corrugation have to be considered. If the corrugation perpendicular to the scattering plane is large, the probability of out-of-plane scattering is high, making in-plane scattering intensity lower. If the corrugation within the scattering plane is large, its angular intensity distribution becomes wider. We first consider the case of end-on collision (P_Z geometry). Since the end of an O_2 molecule collides with the surface, both types of surface

corrugation are larger than those for side-on collision. This accounts for the lowest in-plane direct scattering intensity and the largest peak width for P_Z geometry [Figs. 3(c) and 3(d)].

Second, we discuss the different scattering behaviors between P_X and P_Y geometries. Here, it is important to note that the longitudinal dimension of O_2 is considerably larger than the diameter of the benzene ring of graphite, while the lateral dimension of O_2 is comparable with it [Figs. 3(e) and 3(f)]. O_2 therefore would not feel a large corrugation along the longitudinal direction but feel a larger corrugation along the transverse direction. It is therefore expected that, in P_X geometry where the O_2 axis is perpendicular to the scattering plane, O_2 feels a smaller corrugation perpendicular to the scattering plane but a larger corrugation within the scattering plane than for P_Y geometry. This would cause a larger intensity but a broader width of the in-plane scattering peak for P_X geometry, which is consistent with the observed behaviors. Considering the size of O_2 relative to the benzene ring and the relatively isotropic shape of the benzene ring, similar corrugation difference is expected both along the armchair and zigzag directions [Figs. 3(e) and 3(f)]. This expectation is supported by the fact that similar geometry dependence was observed for O_2 scattering along these two directions on the graphene [Fig. 1(d)]. The presence of the similar geometry dependence for the O_2/HOPG system suggests that the orientation of the graphite domain relative to the scattering plane has little effect on the difference in corrugation between P_X and P_Y geometries.

Raukema *et al.* [28] have shown that the intensity of in-plane O_2 scattering from Ag(110) along [1$\bar{1}$0] azimuth is much lower than that along [001] azimuth. This has been attributed to the fact that O_2 is more easily scattered to the out-of-plane direction if O_2 is incident along the row of surface corrugation. Their explanation is similar to our discussion which associates in-plane scattering intensity with the effective surface corrugation perpendicular to the scattering plane.

TABLE II. Parameters for the O_2 scattering from HOPG at 300 K.

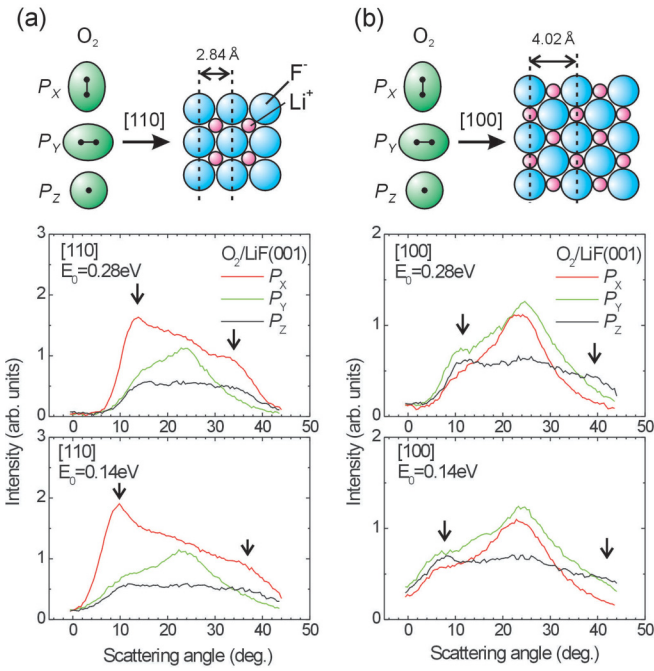| E_0 (eV)	P_X			P_Y			P_Z		
	θ_p (deg)	$\Delta\theta_f$ (deg)	I_D	θ_p (deg)	$\Delta\theta_f$ (deg)	I_D	θ_p (deg)	$\Delta\theta_f$ (deg)	I_D
0.08	23.8	13.1	1.20	23.6	12.7	0.94	24.8	16.4	0.54
0.13	25.3	11.1	1.25	25.3	10.6	1.01	26.0	13.1	0.56
0.18	26.2	9.9	1.25	26.2	9.5	1.03	26.4	11.0	0.63
0.25	26.6	9.2	1.22	26.7	8.7	1.02	26.8	10.2	0.69

FIG. 4. Angular intensity distributions of O₂ molecules scattered from LiF(001) surface along (a) [110] and (b) [100] azimuths derived for P_X, P_Y, and P_Z geometries. The sample temperature is 300 K. Upper and lower panels show the spectra at $E_0 = 0.28$ eV and 0.14 eV, respectively. The scattering spectra are normalized to the intensity of the peak at 20°–30° for random orientation. The arrows indicate the position of the peaks due to the rainbow scattering.

B. Rainbow scattering of O₂ from LiF(100)

To see the effect of surface corrugation on the direct scattering more clearly, we investigated the alignment dependence in O₂ scattering from LiF(001). Figures 4(a) and 4(b) show the alignment dependent O₂ scattering from LiF(001) along [110] and [100] azimuths, respectively. Clear peaks associated with surface rainbow scattering appear at $\theta_f = 9°$ and 36° at $E_0 = 0.14$ eV when O₂ is scattered along the [110] azimuth with its axis perpendicular to the scattering plane (P_X geometry). Intuitively, these rainbow peaks can be understood as the two scattering components coming from the collision with the uphill and downhill part of the surface local corrugation. The rainbow peaks are observed at the same angles also in case of end-on collision although their intensities are much lower. The two peaks approach each other with increasing E_0 similar to the case of Ar scattering from LiF(001) [22,29,30]. In contrast, when the O₂ axis is parallel to the scattering plane (P_Y geometry), the rainbow peaks are strongly attenuated and a peak attributed to the specular scattering ($\theta_f \sim 24°$) is dominant.

These behaviors can be understood based on the O₂ alignment dependence of corrugation. The surface has a square lattice and F⁻ ions with which O₂ mainly interacts are aligned along the [110] and [1$\bar{1}$0] directions. When O₂ is scattered along the [110] azimuth with its axis parallel to the [1$\bar{1}$0] direction, it can feel the surface corrugation strongly, resulting in the surface rainbow scattering similar to that for the scattering of Ne [23] and Ar [22]. However, when the O₂ axis is

parallel to the scattering plane, O₂ cannot feel the corrugation created by surface F⁻ ions because of its elongated shape, making the specular scattering dominant. In case of end-on collision, since O₂ feels the corrugation within the scattering plane, the surface rainbow scattering occurs. Its intensity is however low because O₂ also feels a large corrugation perpendicular to the scattering plane and the out-of-plane scattering probability is high. A small specular scattering peak is seen even in the spectra for P_X geometry. This may be due to the fact that the O₂ axis angular distribution function has a finite angular width.

Figure 4(b) shows that, unlike the O₂ scattering along the [110] azimuth, the rainbow scattering along the [100] azimuth is much weaker and the specular scattering peak is dominant both in P_X and P_Y geometries. This would be due to the fact that, since the O₂ axis is 45° relative to the row of surface F⁻ ions, O₂ cannot feel the surface corrugation effectively. Rainbow scattering appears in the case of P_Z geometry since O₂ feels the corrugation created by F⁻ ions along the [100] azimuth similar to the case of Ar/LiF(001) [22]. The larger separation of the rainbow peaks than along the [110] azimuth reflects the larger distance between neighboring F⁻ ions along the [100] azimuth [22].

C. Energy loss and trapping followed by desorption

The alignment dependence in the energy loss during the O₂-surface collision can be discussed based on the peak position of direct scattering and the trapping probability. The direct scattering peak is located at around $\theta_f = 27°$ ($\theta_i = 18°$) at 110 K [Fig. 3(c)]. Assuming parallel momentum conservation, we can estimate the loss of translational energy to be ∼54%. The fact that the peak position for end-on collision is shifted by ∼1° from that for side-on collision at $E_0 = 0.08$ eV means that the energy loss is 7% larger for end-on collision. The decrease of this peak shift with increasing E_0 suggests that the attractive part of the O₂-graphite surface interaction potential, which becomes more important for collisions at lower E_0, plays an important role in the energy loss process and its geometry dependence causes the observed peak position difference. It might be possible that O₂ approaches the surface more closely and feels a deeper potential well in case of end-on collision. It has been predicted that the rotational excitation of NO is strongly influenced by the attractive part of the interaction potential [14].

Figure 3(c) also shows the alignment dependence of the trapping followed by desorption, the contribution of which is seen at low θ_f region. Its intensity decreases steeply with increasing E_0. Its alignment dependence, although it is not so significant at $E_0 = 0.08$ eV, becomes more clear at higher E_0. The spectra for end-on collision (P_Z geometry) show higher intensities than for the side-on collision (P_X, P_Y), while those for P_X and P_Y geometries exhibit similar intensities. Since thermal O₂ does not stick on HOPG at temperatures >60 K [31], it would be reasonable to assume that the intensity of this feature is proportional to the trapping probability (P_{trap}). Its intensity is much lower at 300 K [Fig. 3(d)].

The larger energy loss observed for end-on collision is consistent with the higher P_{trap} for this geometry [Fig. 3(c)] because efficient energy loss makes trapping easier. The

decrease of P_{trap} with increasing E_0 apparently correlates with that of the peak shift of the direct scattering mentioned above. But, these two quantities may not be directly coupled because similar peak shift with E_0 has been observed also at 300 K, where trapping is much less efficient [Fig. 3(d)]. The larger steric effect in trapping at higher E_0 [Fig. 3(c)] may be understood as follows. P_{trap} decays with E_0 more gradually in the case of end-on collision because O_2 can lose translational energy more efficiently. Therefore, although P_{trap} is similarly high at low E_0, its ratio between the cases of end-on and side-on collision becomes larger with increasing E_0.

IV. CONCLUSIONS

The present alignment-resolved scattering/desorption experiments have clarified that the geometry of an incident homonuclear molecule greatly affects the angular distribution of the scattered molecule, the trapping probability, and the energy dissipation during the molecule-surface collision. Surface corrugation seen by an incident molecule has been shown to be the key to understanding the angular distribution of scattered molecules. Internal state analysis of scattered molecule and/or its theoretical simulation would be useful for further discussions about the origin of the observed geometry dependent energy loss.

[1] A. W. Kleyn, Chem. Soc. Rev. **32**, 87 (2003).

[2] G. O. Sitz, Rep. Prog. Phys. **65**, 1165 (2002).

[3] J. Werdecker, M. E. van Reijzen, B. J. Chen, and R. D. Beck, Phys. Rev. Lett. **120**, 053402 (2018).

[4] O. Godsi, G. Corem, Y. Alkoby, J. T. Cantin, R. V. Krems, M. F. Somers, J. Meyer, G. J. Kroes, T. Maniv, and G. Alexandrowicz, Nat. Commun. **8**, 15357 (2017).

[5] P. R. Shirhatti, I. Rahinov, K. Golibrzuch, J. Werdecker, J. Geweke, J. Altschäffel, S. Kumar, D. J. Auerbach, C. Bartels, and A. M. Wodtke, Nat. Chem. **10**, 592 (2018).

[6] C. Steinsiek, P. R. Shirhatti, J. Geweke, J. A. Lau, J. Altschäffel, A. Kandratsenka, C. Bartels, and A. M. Wodtke, J. Phys. Chem. C **122**, 18942 (2018).

[7] T. J. Curtiss, R. S. Mackay, and R. B. Bernstein, J. Chem. Phys. **93**, 7387 (1990).

[8] M. Okada, Chem. Rec. **14**, 775 (2014).

[9] N. Bartels, K. Golibrzuch, C. Bartels, L. Chen, D. J. Auerbach, A. M. Wodtke, and T. Schäfer, Proc. Natl. Acad. Sci. USA **110**, 17738 (2013).

[10] E. W. Kuipers, M. G. Tenner, A. W. Kleyn, and S. Stolte, Phys. Rev. Lett. **62**, 2152 (1989).

[11] M. G. Tenner, E. W. Kuipers, A. W. Kleyn, and S. Stolte, J. Chem. Phys. **94**, 5197 (1991).

[12] A. W. Kleyn, Prog. Surf. Sci. **54**, 407 (1997).

[13] A. W. Kleyn and T. C. M. Horn, Phys. Rep. **199**, 191 (1991).

[14] C. W. Muhlhausen, L. R. Williams, and J. C. Tully, J. Chem. Phys. **83**, 2594 (1985).

[15] R. J. W. E. Lahaye, S. Stolte, S. Holloway, and A. W. Kleyn, J. Chem. Phys. **104**, 8301 (1996).

[16] M. Kurahashi and Y. Yamauchi, Phys. Rev. Lett. **110**, 246102 (2013); **114**, 016101 (2015).

[17] M. Kurahashi, Prog. Surf. Sci. **91**, 29 (2016).

[18] L. Vattuone, L. Savio, F. Pirani, D. Cappelletti, M. Okada, and M. Rocca, Prog. Surf. Sci. **85**, 92 (2010).

[19] J. N. Greeley, J. S. Martin, J. R. Morris, and D. C. Jacobs, Surf. Sci. **314**, 97 (1994).

[20] R. F. W. Bader, W. H. Henneker, and P. E. Cade, J. Chem. Phys. **46**, 3341 (1967).

[21] T. Kondo, T. Tomii, S. Yagyu, and S. Yamamoto, J. Vac. Sci. Technol. A **19**, 2468 (2001).

[22] T. Kondo, H. S. Kato, T. Yamada, S. Yamamoto, and M. Kawai, J. Chem. Phys. **122**, 244713 (2005).

[23] J. N. Smith, Jr., D. R. O'Keefe, H. Saltsburg, and R. L. Palmer, J. Chem. Phys. **50**, 4667 (1969).

[24] A. C. Wight and R. E. Miller, J. Chem. Phys. **109**, 1976 (1998).

[25] M. Kurahashi and Y. Yamauchi, Rev. Sci. Instrum. **80**, 083103 (2009).

[26] C. Berger, Z. Song, T. Li, X. Li, A. Y. Ogbazghi, R. Feng, Z. Dai, A. N. Marchenkov, E. H. Conrad, P. N. First, and W. A. de Heer, J. Phys. Chem. B **108**, 19912 (2004).

[27] J. Oh, T. Kondo, K. Arakawa, Y. Saito, W. W. Hayes, J. R. Manson, and J. Nakamura, J. Phys. Chem. A **115**, 7089 (2011).

[28] A. Raukema, D. A. Butler, and A. W. Kleyn, J. Phys.: Condens. Matter **8**, 2247 (1996).

[29] S. Miret-Artés and E. Pollak, Surf. Sci. Rep. **67**, 161 (2012).

[30] The analysis with classical perturbation theory [29] has suggested that this rainbow peak approach comes from the E_0 dependent energy transfer from a projectile to a corrugated surface with attractive potential, not from the E_0 dependence of the corrugation [22].

[31] H. Ulbricht, G. Moos, and T. Hertel, Phys. Rev. B **66**, 075404 (2002).